IEEE Access
Multidisciplinary ⋮ Rapid Review ⋮ Open Access Journal

Received 24 January 2025, accepted 15 March 2025, date of publication 24 March 2025, date of current version 4 April 2025.

Digital Object Identifier 10.1109/ACCESS.2025.3554137

RESEARCH ARTICLE

EEG Multi-Mode Oscillatory Brain State Allocation Using Switching Spectral Gaussian Processes

YUNIER PRIEUR-COLOMA[1,2], FELIPE A. TORRES[3], NELSON J. TRUJILLO-BARRETO[4], AND WAEL EL-DEREDY[1,2]

[1]Escuela de Ingeniería Civil Biomédica, Universidad de Valparaíso, Valparaíso 2340000, Chile
[2]Centro Interdisciplinario de Investigación Biomédica e Ingeniería para la Salud (MEDING), Universidad de Valparaíso, Valparaíso 2340000, Chile
[3]Departamento de Computación e Industrias, Universidad Católica del Maule, Talca 3480112, Chile
[4]School of Psychology, Manchester Metropolitan University, M15 6BH Manchester, U.K.

Corresponding author: Yunier Prieur-Coloma (yunier.prieur@uv.cl)

This work was supported by the ANID Chile through the project ANILLO under Grant ACT210053. The work of Yunier Prieur-Coloma was supported by the ANID Chile through the project DOCTORADO NACIONAL under Grant 21221195. The work of Felipe A. Torres was supported by the ANID Chile through the project FONDECYT under Grant 3230682. The work of Wael El-Deredy was supported by ANID Chile through the project FONDECYT under Grant 1241965. The work of Nelson J. Trujillo-Barreto was supported by the Medical Research Council, U.K., under Grant MR/X005267/1.

This work involved human subjects or animals in its research. Approval of all ethical and experimental procedures and protocols was granted by the Scientific and Ethics Committee of AHEPA University Hospital, Aristotle University of Thessaloniki under Application No. 142/12-04-2023.

ABSTRACT We propose a new model for the non-stationary brain state allocation problem from electroencephalography (EEG) data, based on spectral features and their interaction. Spontaneous EEG data are modeled as continuous Gaussian Processes (GPs) emissions governed by discrete states, represented by a hidden semi-Markov model, that switch in time (HsMM-SGP). The GPs are defined by multivariate spectral kernels, covariance functions parameterized in the frequency domain. The multivariate spectral kernels describe oscillatory modes at specific frequencies and their interactions across channels, encapsulating periodicity, amplitude, and spread. Multivariate spectral kernels enable the GPs to represent temporal patterns with fine-grained frequency-specific structures and interactions, a unique spectral "fingerprint" per state, making it particularly suited for capturing non-stationary oscillatory behaviour in the neural time series. The model parameters were estimated using the Expectation-Maximization approach. The inference scheme was validated on data generated from the HsMM-SGP generative model to evaluate the accuracy in recovering the ground truth parameters. Next, we generated time-series from a metastable connectome-connected whole brain network to demonstrate the HsMM-SGP's capability to infer meaningful oscillatory modes that reflect the changes in the underlying dynamics due to varying structural connectivity parameters. Finally, a practical application of the HsMM-SGP is illustrated using EEG data from a healthy control and an AD patient. We show that the inferred brain states exhibit distinct spectral properties across both conditions, with the AD states marked slower frequencies. We conclude that the proposed HsMM-SGP offers a method for estimating physiologically meaningful dynamical brain states.

INDEX TERMS Brain dynamics, Gaussian processes, hidden semi-Markov model, oscillatory brain, spectral mixture kernels.

I. INTRODUCTION

There is growing interest in studying the brain as a dynamical system, focusing on the trajectories by which functional brain networks evolve and transition over time, as well as their

The associate editor coordinating the review of this manuscript and approving it for publication was Angel F. García-Fernández.

dwell times [1], [2]. These dynamics may hold important clues about the reorganization of functional networks [3], [4]. The assumption is that early stages of neurodegeneration could be detected and differentiated from normal aging, even before the presentation of symptoms, through alterations in the dynamical repertoires explored by brain networks, whether at rest or during task performance [5], [6]. Such alterations might manifest as changes in the probability of the brain switching between network configurations, the duration spent in particular configurations, or the sequence or path of these configurations [7], [8]. Brain state allocation refers to the process of identifying recurrent dynamical regimes or modes of operation that generate or explain the quasi-stable patterns of brain activity observed at the levels of topography, sources, or networks [9], [10], [11]. We are interested in identifying physiologically meaningful brain states from electroencephalography (EEG) time-series recorded at the scalp. EEG offers the temporal resolution necessary to identify brain states on fast timescales, capturing resting-state network activations within $\sim$ 50–200 ms [12], [13]. This capability is essential for studying the transient dynamics of neural processes and the temporal reorganization of brain activity.

Methods for brain state allocation include dynamic functional connectivity analysis leverages sliding-window approaches to capture temporal fluctuations in network configurations; Hidden Markov Models (HMMs) and Hidden Semi-Markov Models (HsMM) which provide a probabilistic framework for detecting latent states, their transitions and their durations; and k-means or hierarchical clustering to group similar connectivity patterns into discrete states [14], [15], [16], [17], [18]. With few exceptions, such as [19], [20], and [21], these methods infer brain states based on the band-limited power envelope of the observed time-series. More recently, machine learning approaches, such as deep learning models, have been employed to detect and interpret quasi-stable brain activity patterns across topographical, source, and network levels [13], [22].

On the other hand, oscillatory processes are fundamental to neural coordination and underlie cognitive functions such as attention, memory, and decision-making [3], [4]. These rhythmic activities reflect synchronized electrical patterns that enable different brain regions to interact efficiently [23], [24], [25]. Their interactions are thought to be causal in shaping the brain's functional organization, with oscillatory coupling driving transitions between distinct neural states. For example, theta-gamma coupling facilitates information transfer between local and global networks, influencing cognition and behavior [26], [27], [28]. Disruptions in these dynamics can impair neural communication, contributing to cognitive deficits seen in disorders like Alzheimer's disease and schizophrenia [29], [30]. Analyzing dynamic spectral patterns shows that oscillatory activity shapes neural time series, influencing both network configurations and behavior. Developing brain state allocation methods based on broadband oscillatory activity and its interactions would offer a more physiologically accurate framework, revealing the mechanisms of neural coordination and the dynamics of network transitions. This approach could provide insights into the brain's temporal organization and disruptions in disease, with potential applications in both basic neuroscience and clinical settings. Methods to identify dynamical spectral patterns in brain activity have been proposed. One approach extracts modes by analyzing the cross-correlation of signals within backward time windows, but typically applies band-pass filtering, limiting the analysis to specific frequency ranges [31]. Dynamic Mode Decomposition similarly identifies modes corresponding to distinct frequencies within signals [32], [33], but these modes are typically unimodal in frequency, limiting their ability to capture interactions between networks operating at different frequencies [34].

We propose that Gaussian Processes (GPs) provide a flexible framework for identifying dynamic spectral patterns in brain activity, capturing complex temporal relationships without relying on predefined frequency bands [35]. Using spectral kernels, GPs model covariance functions in the frequency domain, enabling the inference of latent oscillatory properties of the data across different frequency bands. Multivariate spectral kernels extend this approach to capture statistical interdependencies across observations from multiple channels [36], [37]. These interdependecies are modeled through cross-covariance functions with meaningful spectral parameters [38], [39].

In this paper, we propose a new model for the non-stationary brain state allocation problem based on spectral features and their interactions across multiple channels. While broadly applicable to any electrophysiological data modality, we focus here on EEG due to its non-invasive nature, high temporal resolution, ability to capture fast neural dynamics, and broad brain coverage. The proposed framework models EEG data as emissions from GPs with multivariate spectral kernels, each corresponding to a discrete brain state, with state transitions governed by a HsMM. Consequently, each state is associated with a unique set of spectral parameters that characterize fine-grained properties of oscillatory modes (e.g., fundamental frequency, amplitude, and phase shift) underlying the interactions among multiple channels.

The contribution of this paper is the development of a physiologically interpretable framework for representing underlying oscillatory dynamics by identifying brain states with unique spectral fingerprints derived from broadband activity. Our proposal offers a comprehensive characterization of oscillatory dynamics, which could enhance our understanding of neural coordination and transitions between brain states, with potential applications in both normal brain function and disease detection.

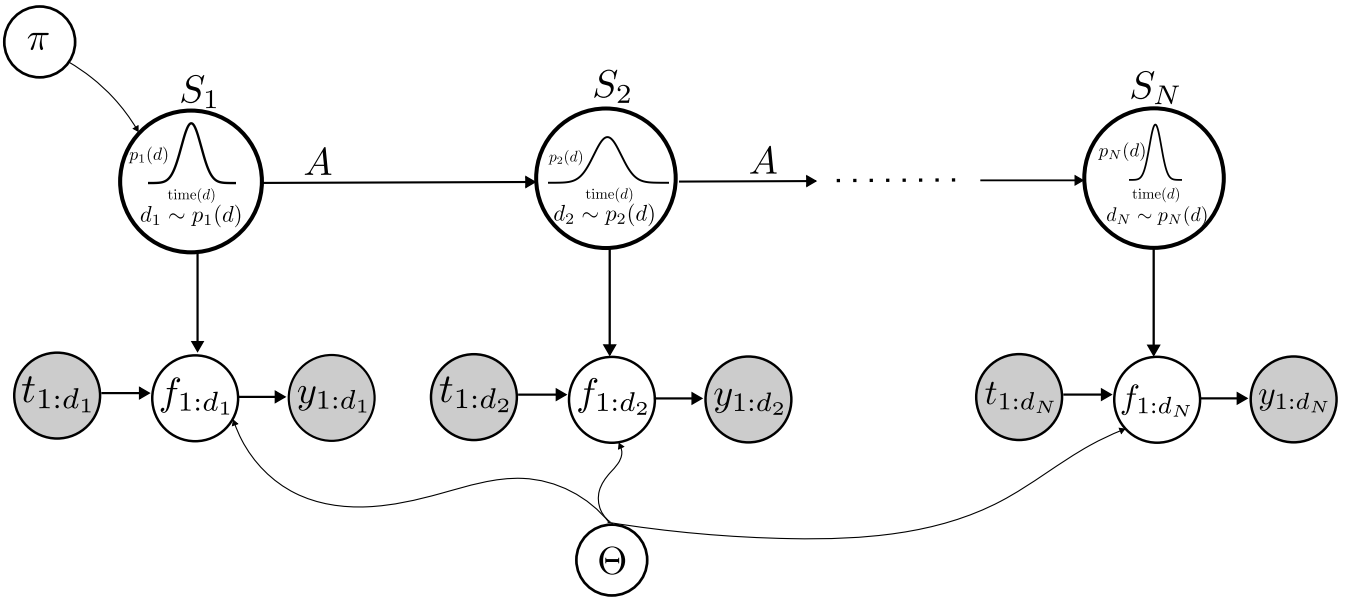

FIGURE 1. Graphical model of the HsMM with spectral Gaussian Process emissions. The proposed model assumes that a sequence of discrete latent states governs the observed data across *C* channels. Each state is associated with a Gaussian Process emission model with multivariate spectral kernels, defining the statistical properties of the observations. The segment lengths are governed by a duration distribution specific to each state, and the time series is divided into *N* segments, each corresponding to a latent state.

II. MATERIALS AND METHODS

A. HIDDEN SEMI-MARKOV MODEL WITH SPECTRAL GAUSSIAN PROCESSES EMISSIONS

The proposed method is based on recent advances in GPs with spectral kernels and HsMM theory. We assume that observations from C channels are generated by a sequence of discrete latent states. Each state is represented by a GP using a multivariate spectral kernel, while both the states and their durations (i.e., the time segment during which a state remains active) are treated as latent variables. We capitalize on the flexibility of HsMM models by modeling the duration of states using probability distributions.

The multivariate time series $\boldsymbol{Y} \in \mathbb{R}^C$, corresponding to C channels, is divided into N segments, where each segment $\{\boldsymbol{y}_n\}_{n=1}^N$ is governed by a latent state $\{S_n\}_{n=1}^N$. Each segment consists of observations $\{y_t\}_{t=1}^{d_n}$, indexed by a set of time inputs $\{t_i\}_{i=1}^{d_n}$, where d_n represents the duration during which state S_n remains active. The latent function $\{f_t\}_{t=1}^{d_n}$, responsible for generating the observations, is modeled using GPs with multivariate spectral kernels. Fig. 1 depicts the described generative model.

As shown in Fig. 1, quasi-stationary time segments in the observed data are represented according to the properties of the associated GP. In the next subsections, a brief description of the GPs theory is provided. For more details on the HsMM and the GPs used here the reader is referred to [35], [37], [40], and [41], respectively.

B. GAUSSIAN PROCESSES

GPs are a non-parametric probabilistic modeling approach used in machine learning for regression, classification, and uncertainty estimation tasks [35]. It provides a powerful framework for discovering hidden patterns and underlying correlations in data. This work focuses on the analysis of time series; hence, we employ GPs defined over time. Formally, a GP is defined as follows:

Definition 1 (Gaussian Process): A Gaussian Process is a real-valued stochastic process $f(t)$ over an input set $\boldsymbol{t}$ such that for any finite subset of inputs $\{t_i\}_{i=1}^T \subset \boldsymbol{t}$, the set of random variables $\{f(t_i)\}_{i=1}^T$ follows a multivariate Gaussian distribution.

From a function-space perspective, GPs define distributions over functions fully specified by a mean function $m(t) = \mathbb{E}[f(t)]$, commonly assumed $m(t) = 0$, and a covariance function or kernel $k(t, t') = \text{cov}(f(t), f(t'))$. In realistic modeling scenarios, the true function values are not directly accessible. Instead, only noisy observations are available, expressed as $y = f(t) + \epsilon$, where ϵ is commonly assumed to be additive, independent, and identically distributed Gaussian noise.

Typically, modeling tasks using GPs involve the specification of a hierarchical model. At the first level, there is a set of possible kernel structures $\mathcal{S}_i$. At the second level are hyperparameters Θ which control the shape of the structure at the first level. For example, the squared-exponential kernel has the following structure:

$$k(t, t'; \Theta) = \sigma_f^2 \exp\left(-\frac{1}{2l^2}(t - t')^2\right) \tag{1}$$

where $\Theta = \left\{\sigma_f^2, l\right\}$. Here σ_f^2 and l represent the signal variance and the length scale, respectively. Briefly, the signal variance is interpreted as the process energy, while the

length scale can be interpreted as the process memory—the number of time units required to move away from t' to have completely uncorrelated samples. Training GPs involves estimating the hyperparameters from observed data, providing interpretable parameters that reflect the properties of the data.

Next, a formulation is presented that aims to replace the a priori selection of the $\mathcal{S}_i$ structure by designing a flexible kernel based on the data.

1) SPECTRAL MIXTURE KERNEL

A stationary kernel is a function of $\tau = t - t'$. Thus, it is invariant under translations in the input space [35]. In the context of time series analysis, τ represents a temporal lag. Any stationary kernel can be represented according to Bochner's theorem [42], which establishes the following:

Theorem 1 (Bochner's theorem): A complex-valued function k on $\mathbb{R}^P$ is the covariance function of a weakly stationary mean square continuous complex-valued random process on $\mathbb{R}^P$ if and only if it can be represented as:

$$k(\tau) = \int_{\mathbb{R}^P} e^{j\omega\tau} S(\omega) d\omega \tag{2}$$

where $S(\omega)$ is known as the spectral density corresponding to k.

Bochner's theorem provides the following explicit relationship between the spectral density $S(\omega)$ and the covariance function $k(\tau)$:

$$k(\tau;\Theta) = \int S(\omega) e^{j\omega\tau} d\omega \tag{3}$$

$$S(\omega) = \int k(\tau) e^{-j\omega\tau} d\tau \tag{4}$$

From (3) and (4), it can be observed that the spectral density determines the stationary kernel properties. The most popular kernels in machine learning fields include the squared exponential, rational quadratic, Mátern class, and mixtures of them [35], [43]. However, these kernels represent only a small subset of stationary kernels, as their spectral density corresponds to a Gaussian centered at the origin. To overcome this limitation, Wilson et al. [41] proposed modeling the spectral density $S(\omega)$ as a weighted mixture of M-Gaussians, centered at $\mu^{(m)}$, with variances $v^{(m)}$ and weights $w^{(m)}$ as follows:

$$S(\omega) = \sum_{m=1}^{M} w^{(m)} \frac{1}{\sqrt{2\pi v^{(m)}}} \exp\left(-\frac{1}{2v^{(m)}}(\omega - \mu^{(m)})^2\right) \tag{5}$$

The kernel associated with the spectral density in (5) is referred to as the spectral mixture kernel:

$$k(\tau;\Theta) = \sum_{m=1}^{M} w^{(m)} \exp\left(-\frac{1}{2} v^{(m)} \tau^2\right) \cos(\mu^{(m)}\tau) \tag{6}$$

The spectral mixture kernel is able to approximate any stationary kernel with arbitrary precision, using a spectral representation with a sufficient number of mixture components. Thus, it provides a flexible framework for capturing the appropriate statistical structure that characterizes univariate time series. However, the analysis of brain activity inherently involves multivariate time series. At the source level, there is interaction among neuronal populations distributed in different brain regions. At the sensor level, the electrical activity generated by these sources is extracranially detected using a sensor array. Therefore, for brain activity modeling, schemes that capitalize on the statistical interdependencies in the multivariable time series are desirable.

2) SPECTRAL MIXTURE KERNELS FOR MULTI-OUTPUT GAUSSIAN PROCESSES

Multi-output GPs are a multivariate extension that assembles C-different GPs, allowing the modeling of the statistical interdependence between time series [44]. Multi-output GPs lead to a vector-valued process:

$$\boldsymbol{f}(t) \sim \mathcal{GP}(\boldsymbol{m}(t), \boldsymbol{K}(t, t')) \tag{7}$$

where $\boldsymbol{m}(t) \in \mathbb{R}^C$ is a vector with elements that are the mean functions $\{m_c(t)\}_{c=1}^{C}$ of each output. The covariance function $\boldsymbol{K}(t, t')$ represents the correlation between the outputs $f_c(t)$ and $f_{c'}(t')$ and is defined as:

$$\boldsymbol{K}(t, t')_{c,c'} = k_{c,c'}(t, t') = \text{cov}(f_c(t), f_{c'}(t')).$$

Given a set of input points $\boldsymbol{X}$ of length T, the prior distribution over $\boldsymbol{f}(\boldsymbol{X})$ is given by:

$$\boldsymbol{f}(\boldsymbol{X}) \sim \mathcal{GP}(\boldsymbol{m}(\boldsymbol{X}), \boldsymbol{K}(\boldsymbol{X}, \boldsymbol{X})) \tag{8}$$

where $\boldsymbol{m}(\boldsymbol{X})$ is a TC vector resulting from concatenating the mean vectors of each output, and $\boldsymbol{K}(\boldsymbol{X}, \boldsymbol{X})$ is a $TC \times TC$ block-partitioned matrix with the following form:

$$\boldsymbol{K}(\boldsymbol{X}, \boldsymbol{X}) = \begin{bmatrix} \boldsymbol{K}(\boldsymbol{X}_1, \boldsymbol{X}_1) & \cdots & \boldsymbol{K}(\boldsymbol{X}_1, \boldsymbol{X}_C) \\ \boldsymbol{K}(\boldsymbol{X}_2, \boldsymbol{X}_1) & \cdots & \boldsymbol{K}(\boldsymbol{X}_2, \boldsymbol{X}_C)) \\ \vdots & \ddots & \vdots \\ \boldsymbol{K}(\boldsymbol{X}_C, \boldsymbol{X}_1) & \cdots & \boldsymbol{K}(\boldsymbol{X}_C, \boldsymbol{X}_C) \end{bmatrix} \tag{9}$$

where each block $\boldsymbol{K}(\boldsymbol{X}_c, \boldsymbol{X}_{c'})$ is a $T \times T$ matrix comprising the covariances between channels c and c'. We note here that the dimensionality of $\boldsymbol{K}$ will have consequences on the scalability to time series with high density channels (Section II-D2).

Multivariate kernels jointly model the covariance functions within each region (diagonal elements in $\boldsymbol{K}$) and the cross-covariance functions between regions (off-diagonal elements in $\boldsymbol{K}$) in multi-output GPs. Multivariate spectral kernels extend the concept of the spectral mixture kernel to model covariance functions using spectral densities and cross-covariance functions using cross-spectral densities [36]. We capitalize on the multivariate spectral kernels' potentials to capture the oscillatory modes and their properties across multiple channels, simultaneously. In this work, we focus on the Cross-Spectral Mixture (CSM) kernel to model the cross-covariance functions between channels [37]. The CSM kernel has a biophysically consistent formulation, assuming that the channels share a set of

oscillatory modes. It defines the cross-covariance function between two channels $c, c' \in \{1, \ldots, C\}$ as follows:

$$k_{c,c'}(\tau;\Theta) = \sum_{m=1}^{M} \sqrt{w_c^{(m)} w_{c'}^{(m)}} \exp\left(-\frac{1}{2}\nu^{(m)}\tau^2\right) \times \cos\left(\mu^{(m)}(\tau + \phi_{c'}^{(m)} - \phi_c^{(m)})\right) \quad (10)$$

where $\Theta = \{w_i^{(m)}, \mu^{(m)}, \nu^{(m)}, \phi_i^{(m)}\}$ represents the kernel hyperparameters. From (10) can be observed that the CSM kernel comprises the linear combination of M-oscillatory modes, and its hyperparameters provide a plausible description of each one: $\mu^{(m)}$, $\nu^{(m)}$, $w_i^{(m)}$ and $\phi_i^{(m)}$ represent for the m-mode the fundamental oscillatory frequency, the inverse length-scale of each m-mode, covariance's magnitude and phase of the i-channel, respectively. In this work, we use multi-output GPs with CSM kernels as the emission model within the HsMM framework. We hypothesize that this emission model will provide meaningful insights into the spectral properties of spontaneous brain activity, distinguishing between healthy and pathological conditions.

C. EMISSION MODEL BASED ON SPECTRAL GAUSSIAN PROCESSES

Here, the emission model is formally defined. Segment observations $\boldsymbol{y}_n \in \mathbb{R}^C$, corresponding to C channels, are modeled as emissions from a HsMM with Z latent states. Each state S_i, where $i \in \{1, \ldots, Z\}$, is associated with a specific set of spectral kernel hyperparameters, Θ_i. The latent state assignment $S_n = i$ indicates that the i-th state controls the emissions at the n-th time segment through the corresponding set of GPs parameters:

$$\boldsymbol{y}_n^i \sim \mathcal{N}\left(\boldsymbol{f}^i(t), \boldsymbol{\Lambda}\right), \quad \boldsymbol{f}^i(t) \sim \mathcal{GP}\left(\boldsymbol{0}, \boldsymbol{K}(t, t'; \Theta_i)\right) \quad (11)$$

where $\boldsymbol{K}(t, t'; \Theta_i)_{c,c'} = k_{c,c'}(t, t'; \Theta_i)$ represents the correlation between the observations from channels c and c' at time points t and t', respectively; and $\boldsymbol{\Lambda}$ is the noise covariance matrix. The noise term is assumed to be independent of the GP and represents the observation noise across all time segments. Consequently, quasi-stationary segments in EEG data are assigned to a latent state i, each characterized by a unique set of spectral parameters Θ_i, which encapsulate the properties of the oscillatory modes across the C channels.

D. HSMM-SGP INFERENCE

Commonly, in HsMM models, observations are assumed to be conditionally independent for given states, that is, $P(\boldsymbol{y}_{t-d:t}|S_{t-d:t} = j) = \prod_{t=1}^{d} p(\boldsymbol{y}_t|S_t = j)$ [9]. However, our emission model conception imposes time segments with correlated samples according to the associated kernel. As shown in Fig. 1, time points belonging to a time segment exhibit dependency ($\boldsymbol{y}_{t-1,2,\ldots,d} \rightarrow \boldsymbol{y}_t$).

For the HsMM-SGP inference, an Expectation-Maximization (EM) iterative procedure is used. The Expectation-step involved sampling observation time segments and their corresponding states jointly, using the Forward Filtering and Backward Sampling algorithm. Afterward, HsMM-SGP parameters are updated using the observations and states sampled in the previous Expectation step. The proposed EM procedure is presented in Algorithm 1.

Algorithm 1 Expectation-Maximization Algorithm

```
Initialize parameters: A, π, Θ
repeat
    Expectation Step:
    //Compute forward variable
    α ← Forward_Filtering(data, A, π, Θ)
    //Perform backward sampling
    (y_1, ..., y_N), (S_1, ..., S_N) ← Backward(α)
    Maximization Step:
    A, π, Θ ← Update((y_1, ..., y_N), (S_1, ..., S_N))
until Convergence
```

Next, the forward filtering and backward sampling algorithms are introduced, as they are crucial components of the proposed EM procedure outlined in Algorithm 1.

1) FORWARD FILTERING AND BACKWARD SAMPLING

During the Expectation step, the observation segments and their corresponding states are jointly sampled. Our assumption that observed time series ($\boldsymbol{Y}$) are divided into N time segments, such that each segment $\{\boldsymbol{y}_n\}_{n=1}^N$ has an associated responsible state $\{S_n\}_{n=1}^N$, as shown in Fig. 1 it can be expressed as $P(\boldsymbol{Y}, S) \sim (\boldsymbol{y}_1, \ldots, \boldsymbol{y}_N), (S_1, \ldots, S_N)$. For an observed time series $\boldsymbol{Y}$ and model parameters $\lambda = \{A, \pi, \Theta\}$, segments and states' sampling involve computing probabilities marginalizing the joint distribution $P(\boldsymbol{Y}, S|\lambda)$ over all possible state sequences, resulting in a demanding computational task [40]. To efficiently sample the time segments ($\boldsymbol{y}_n$) and their responsible states (S_n), the forward-filtering and backward sampling algorithms are used [45]. During forward filtering the joint probability that time segment $\boldsymbol{y}_{t-d:t}$ has started d samples before time step t and belongs to state j is computed. The forward filtering variable is computed as follows:

$$\alpha(t, j, d) = P(\boldsymbol{Y}_{t-d:t}|S_{t-d:t} = j, \Theta) \times \sum_{h=1}^{D}\sum_{i=1}^{L} \alpha(t-d, i, h) P(j|i, A) \quad (12)$$

where, D and L represent the maximum duration of the segments and the number of states, respectively. $P(\boldsymbol{Y}_{t-d:t}|S_{t-d:t} = j, \Theta)$ represents the probability that the time segment $O_{t-d:t}$ was generated from state j, and it is computed as:

$$P(\boldsymbol{Y}_{t-d:t}|S_{t-d:t} = j, \Theta) = P(\boldsymbol{Y}_{t-d:t}|\mathcal{GP}_j) p_j(d) \quad (13)$$

where, $p_j(d)$ represents the duration distribution of state j.

The forward variable is initialized as $\alpha(1, :, j) = \pi p_j(d)$, and if $t - h \leq 0$ it is kept as $\alpha(t, :, :) = 0$. Forward

probabilities $\alpha(t, j, d)$ are recursively computed according to (12).

In high-dimensional probability distributions, likelihood values typically decrease as the dimensionality increases. This decline complicates statistical inference and model fitting, as the resulting values can become so small that they are often difficult to represent accurately on standard computing systems. This phenomenon is particularly relevant in the context of GPs, where it limits the calculation of emission probabilities $P(\boldsymbol{Y}_{t-d:t}|S_{t-d:t} = j, \Theta)$ presented in (13). To address this limitation, both emission probabilities and forward probabilities are computed in logarithmic space (see *Supplementary Material A*).

Afterwards, the time segments $(\boldsymbol{y}_n)$ and states S_n are sampled based on the forward variable α. Backward sampling starts from the last time step and moving towards the first, that is, for $t = T$ and from $(d_N, j) \sim argmax_{d,j}\alpha(t, j, d)$, the time segment is defined as $\boldsymbol{y}_N = \boldsymbol{Y}_{t-d_N:t}$ and its responsible state $S_N = j$. Next, the time segment and the associated state are defined from $(d_{N-1}, j) \sim argmax_{d,j}\alpha(t - d_N, j, d)$. This procedure is performed until $t = 1$, providing the time segments and their corresponding states $(\boldsymbol{y}_1, \ldots, \boldsymbol{y}_N), (S_1, \ldots, S_N)$. Backward sampling is presented in Algorithm 2.

Algorithm 2 Backward Sampling

```
t = T; n = N
while t > 0 do
    (d, j) ~ argmax_{d,j} α(t, j, d)
    //Sampling segment and state
    y_N = Y_{t-d:t}; S_n = j
    //Update time instant and segment label
    t = t − d; n = N − 1
return (y_1, ..., y_N), (S_1, ..., S_N)
```

The procedure for updating the parameters of the HsMM-SGP model, corresponding to the maximization step outlined in Algorithm 1, is now presented.

2) HSMM-SGP PARAMETERS UPDATE

In the Maximization step, the parameters A, π, and Θ are updated using the sampled segments and their responsible states from the previous Expectation step. The probability of transitioning from state i to state j is computed based on the sampled segment sequence as follows:

$$P(j|i) = \frac{\xi_{ij} + \beta}{\xi_i + Z\beta} \tag{14}$$

where ξ_{ij} is the number of transitions from state i to state j, ξ_i is the total number of transitions from state i, β is the smoothing parameter (set to $\beta = 0.1$), and Z is the total number of states. Subsequently, the parameters of the duration probability and CSM kernel hyperparameters of each state are estimated using the length of assigned segments and maximizing the log-likelihood function via the Adam optimizer, respectively.

The log-likelihood is expressed as follows:

$$\log p(\boldsymbol{y}|\Theta) = -\frac{1}{2}\boldsymbol{y}^T\boldsymbol{K}^{-1}\boldsymbol{y} - \frac{1}{2}\log|\boldsymbol{K}| - \frac{TC}{2}\log 2\pi \tag{15}$$

The terms of the log-likelihood have the following roles, $-\boldsymbol{y}^T\boldsymbol{K}^{-1}\boldsymbol{y}/2$ is the data fit; $\log|\boldsymbol{K}|/2$ is the complexity penalty, and $TC\log 2\pi/2$ is a normalization constant. Hence, the maximizing log-likelihood naturally provides a trade-off between model fit and complexity. The inversion of $\boldsymbol{K}$ in (15) demonstrates the channel scalability problem.

E. EXPERIMENTS

To assess the capabilities of the proposed model, experiments were conducted using three different datasets:

1) GROUND TRUTH DATA

Ground truth data was generated using the HsMM-SGP generative model, as shown in Fig. 1. The purpose of this experiment was to verify that the inference scheme recovers the known model parameters that generated the data.

2) SIMULATED BRAIN-LIKE NETWORKS

Brain-like networks were simulated using connectome-coupled Kuramoto oscillators and biophysical parameters, such as global coupling and mean delay. Simulations were performed with two different sets of biophysical parameters, resulting in data with distinct spectral properties that reflect different network dynamics. Then, it was evaluated whether the model accurately captured changes in the oscillatory dynamics driven by variations in the biophysical parameters.

3) EEG DATA

The model was used in a practical application with EEG data from a healthy control (HC) and an Alzheimer's disease (AD) patient to evaluate its ability to distinguish the oscillatory properties underlying brain dynamics in both healthy and neurodegenerative conditions.

III. RESULTS

In this section, the results of the experiments conducted using ground truth data, simulated brain-like networks, and EEG data are presented.

A. PARAMETER INFERENCE VALIDATION USING GROUND TRUTH DATA

The goal of the ground truth experiment was two-fold: first to validate the model's duration inference; and second, to demonstrate that the inference scheme recovers the observation model used to generate the data, as ground truth is unknown for EEG data.

The data were generated based on the model shown in Fig. 1, using three states with known parameters. States' durations were simulated using Normal distributions, and transition matrices were randomly generated by sampling their elements from a uniform distribution over the interval $[0, 1)$. Subsequently, each row of the matrix

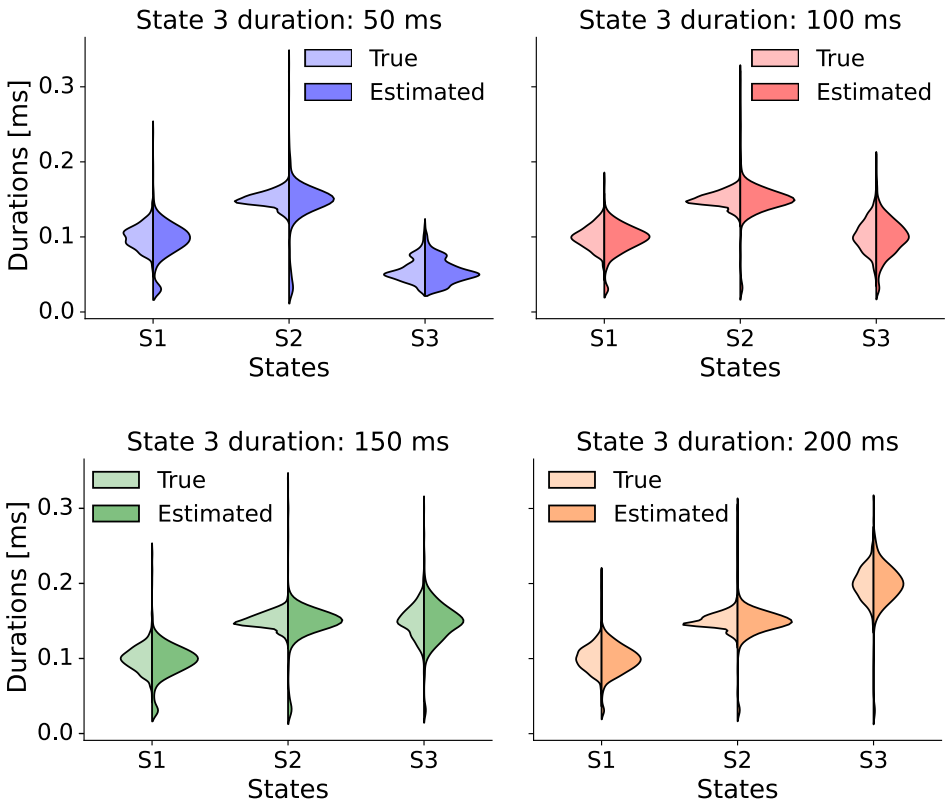

FIGURE 2. Validation of the recovery of duration distributions using ground truth data. Samples from an HsMM-SGP with three states were generated where states 1 and 2 had fixed mean durations, while state 3 varied. For each run, 10 independent state time courses were drawn.The figures illustrate density curves of the distributions of the true and the model-estimated durations.

was normalized such that the sum of its elements sum to 1. These procedures were applied to all simulations.

In the first stage, the procedure presented in [9] was followed to evaluate the model's ability to recover the state time course for states with different durations. The state's durations $p_n(d)$ were modeled using Normal distributions for both the data generation and inference process. Similar to the approach presented by Ulrich et al. [37], time series were simulated considering three states in two channels. The mean duration distributions of two states were fixed ($\mu_{S_1} = 100$ ms, $\sigma_{S_1} = 15$ ms; $\mu_{S_2} = 150$ ms, $\sigma_{S_2} = 10$ ms), while the mean duration of the third state was systematically varied from 50 ms to 200 ms, with $\sigma_{S_3} = 20$ ms. Each state was characterized by a CSM kernel with a single oscillatory mode but different fundamental frequencies: state 1 ($\mu = 4$ Hz), state 2 ($\mu = 10$ Hz), and state 3 ($\mu = 25$ Hz). The inverse length-scale was set to $\nu = 1$ Hz^2 for all states. The quasi-stationary segments associated with each state were obtained by randomly sampling from the GP specified by the covariance matrix $\boldsymbol{K}$, using a temporal grid with a sampling frequency of 200 Hz. For each duration of the state 3, 10 independent state sequences were generated using the HsMM-SGP with the ground truth parameters. For each sequence, an HsMM-SGP was trained to infer the corresponding parameters.

The order of the states' labels in the generated data was arbitrary; therefore, the estimated states were matched to the ground truth states using the affine-invariant Riemannian distance (AIRD) between their respective covariance matrices as dissimilarity metric between the states. After matching the states, the correlation and normalized Hamming distance between the estimated state time course and the ground truth state time course were computed (see *Supplementary Material B*).

Fig. 2 shows density curves representing the distributions of true and model-estimated durations for states with varying mean durations. The proposed scheme was able to estimate the states' duration distributions accurately for states with short, intermediate, and long durations. This confirmed that the inference scheme recovered states with durations like those observed in EEG data.

In the second stage, the ability of the proposed model to estimate the proportion of oscillatory modes within the channels of simulated states was evaluated. Three brain states were simulated across four channels, with each state comprising 3 oscillatory modes ($M = 3$). Each state was dominated by a primary oscillatory mode within a specific frequency band (θ [4-8 Hz], α [8-13 Hz], or β [13-30 Hz]), while the remaining two modes corresponded to distinct frequency bands. The proportion of each m-th mode in the c-th channel was defined using the parameter $w_c^{(m)}$, and

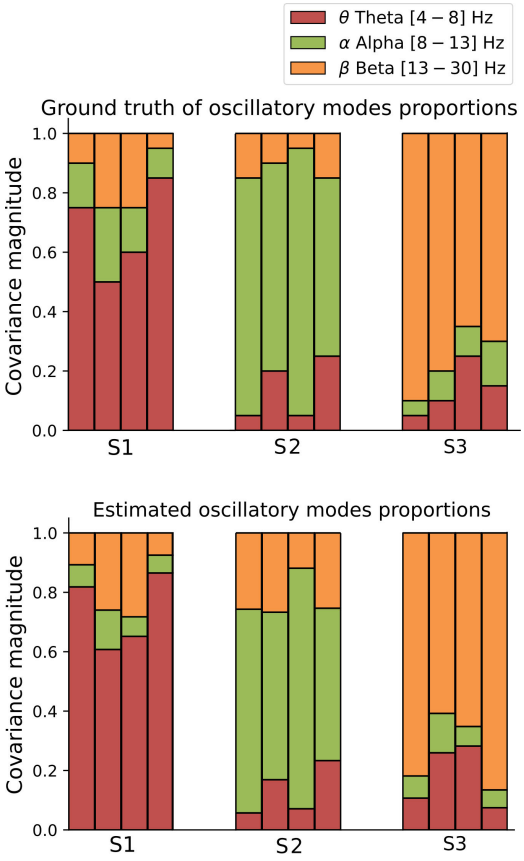

FIGURE 3. Results from ground truth data recovering the proportion of oscillatory modes associated with three simulated states (four regions per state). Top: the ground truth proportions of oscillatory modes for state 1 (S1), state 2 (S2), and state 3 (S3), with predominant fundamental frequencies at theta, alpha, and beta bands, respectively; Bottom: the estimated oscillatory modes proportions for each state.

$\nu^{(m)} = 1$ Hz^2 was set for all modes, with phase differences $(\phi_{c'}^{(m)} - \phi_c^{(m)})$ predefined.

Fig. 3 presents the results from the ground truth data experiment, showing the estimation of the proportions of oscillatory modes across channels in the simulated states. Notably, the dominant oscillatory mode in each state was recovered by the model, reflecting its capacity for capturing the underlying structure of oscillatory activity. This highlighted the model's sensitivity to the predominant frequency bands in each state, while simultaneously estimating the contribution of secondary modes across channels, thereby considering the richness of oscillatory dynamics.

B. SIMULATED BRAIN-LIKE ACTIVITY DATA

By brain-like activity refers to complex dynamics emerging from interacting oscillators that represent neural populations [46], [47]. Brain-like activity was simulated using a network of Kuramoto oscillators coupled according to the Automatic Anatomic Labeling (AAL90) parcellation and tractography [48]. Each brain region was represented as an oscillator with a natural frequency, and it interacted with the others by a sinusoidal function of the delayed phase difference as follows:

$$\dot{\phi}_i(t) = \omega_i + W \sum_j c_{ij} sin(\phi_j(t - d_{ij}) - \phi_i(t)) \qquad (16)$$

where $\phi_i(t)$ is the phase of the i-th brain region with natural frequency ω_i (set at 40 Hz for all regions); c_{ij} denotes the connection strength between regions i and j; and W and d_{ij} are, respectively, the global scale parameter influencing all connections and the conduction delay between the i-th and j-th regions.

We simulated two brain conditions (to emulate healthy and disease cases) with multiple oscillatory states using the Kuramoto model's global parameters: global coupling and mean conduction delay (MD), following the approach outlined in [49]. The conditions had the same global coupling but different mean conduction delay. Specifically, the points in the biophysical parameter space corresponding to each condition were set as follows: Cond1) $W = 4.5$, $MD = 18$ ms; and Cond2) $W = 4.5$, $MD = 23$ ms. The simulated activity was sampled at 200 Hz, and the first 21 seconds were discarded to avoid transient events.

To ensure the tractability of the inversion of $\boldsymbol{K}$ (see (15)), 10 out of the AAL90 atlas regions were selected. The selection was based on the regions similarity to the average PSD, such that they represented the global oscillatory dynamics.

During the HsMM-SGP inference process, four latent states were chosen. Each latent state was configured with three oscillatory modes ($M = 3$) for Cond1 and four oscillatory modes ($M = 4$) for Cond2. This selection was based on the peaks of the average PSD of the simulated neural activity. Each latent state was represented by a kernel that provided parameters reflecting the cross-spectra between each pair of channels at specific oscillatory modes. To represent each state, the average amplitude of all cross-spectra across channel pairs was calculated.

Fig. 4 presents the results of the simulated brain-like networks with two parameter sets leading to distinct spectral features. The top panel presents the PSD of the 10 selected regions and the average PSD across the 90 regions defined by the AAL90 atlas, illustrating how differences in mean conduction delay influence the spectral power distribution. The bottom panels present the inferred multi-mode oscillatory brain states, capturing activity across different frequency bands and providing a characterization of the oscillatory dynamics emerging from network synchronization driven by the biophysical parameters.

C. EEG DATA EXPERIMENT

The EEG experiment aimed to test whether the model's parameters could plausibly distinguish the oscillatory properties underlying brain dynamics in healthy and neurodegenerative conditions. Publicly available resting-state EEG data from an Alzheimer's disease (AD) patient (female, 61 years old) and a healthy control (HC) subject (male, 57 years old) were used, as provided by Miltiadous et al. [50].

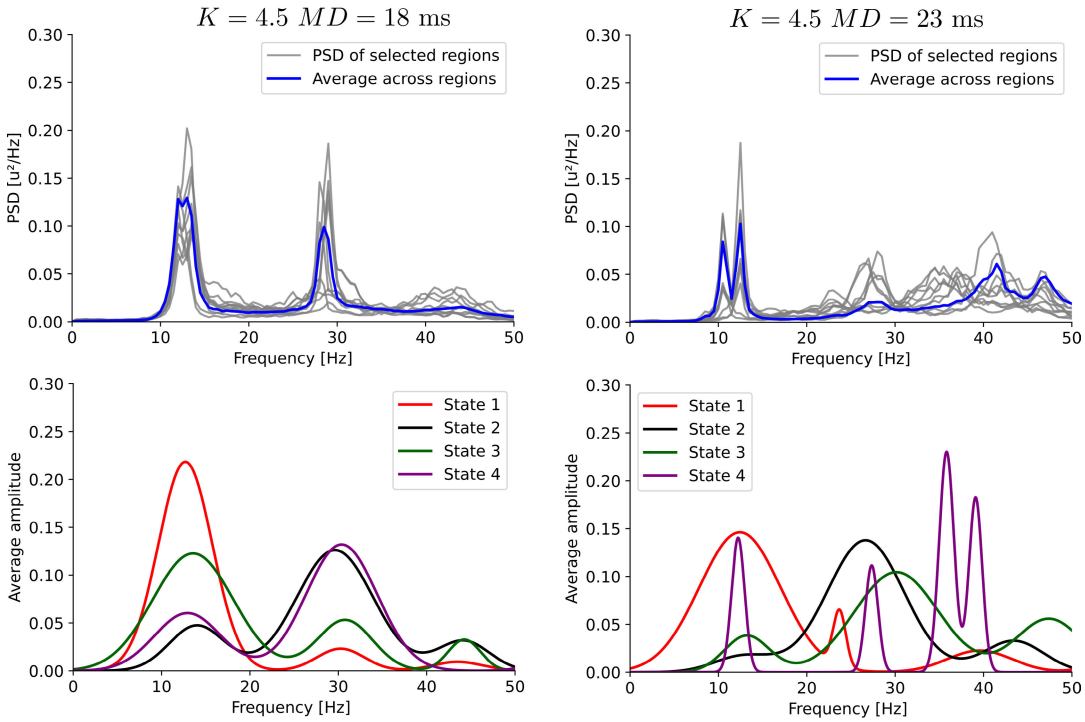

FIGURE 4. Simulation of multiples oscillatory states from Kuramoto oscillator models with two sets of biophysical parameters (W, MD), and their recovery by HsMM-SGP. Top: average PSD across the AAL90 atlas regions (blue line), and the PSDs of the 10 selected regions for the HsMM-SGP inference process. The PSDs highlight the dominant frequency peaks across regions for each configuration. Bottom: multi-mode oscillatory brain-like states inferred by the HsMM-SGP. The modes of each state are represented by the average amplitude of the cross-spectra over channel pairs.

The recordings were obtained with 19 electrodes positioned according to the 10–20 international system, while the subjects had their eyes closed. The sampling rate was 500 Hz, and each recording lasted approximately 13 min. After acquisition, the data were bandpass filtered between 0.5 and 45 Hz, and artifacts were removed. As described in the original work [50], the participants provided their informed consent to participate in the study. The experimental procedure was approved by the Scientific and Ethics Committee of AHEPA University Hospital, Aristotle University of Thessaloniki, under protocol number 142/12-04-2023, and adhered to the principles outlined in the Declaration of Helsinki.

For the inference, the data were downsampled to 200 Hz, and a 4 Hz high-pass filter was applied. Five minutes of recordings were used from 10 channels (Fp1, Fp2, F1, F2, C3, C4, P3, P4, O1, and O2), which cover the frontal, central, parietal, and occipital regions of the scalp.

In EEG data, the number of latent states and the number of oscillatory modes are unknown a priori. The HsMM-SGP was implemented using four states ($Z = 4$) in line with the canonical EEG microstates [7], [12]. The spectral kernel associated with each state was configured to include six oscillatory modes ($M = 6$) based on the Akaike Information Criterion (AIC) (see *Supplementary Material C*).

Fig. 5 presents the inferred multi-mode oscillatory brain states for the HC subject and the AD patient. The inferred states exhibited distinct spectral properties between the HC subject and the AD patient. The states were dominated by oscillatory modes within specific frequency bands, including θ, α, β, and γ [30-100 Hz], and contained background modes within these canonical bands. It is worth noting that the states were inherently non-comparable across subjects; however, these differences might reflected variations in underlying brain activity. As shown in Fig. 6, the α state in the AD patient exhibited a longer duration compared to that in the HC subject.

It has been shown that intrahemispheric and interhemispheric coherence reflects changes in neural connectivity, which is of cognitive and clinical relevance, particularly in the context of neurodegenerative diseases [51]. The CSM kernel inherently provides the cross-spectrum between each pair of channels. Although the cross-spectrum does not directly represent coherence, its magnitude can be interpreted as an indicator of coherence at specific frequencies.

Fig. 7 presents the cross-spectrum for the labeled state β of the HC subject for a subset of frontal (F3 and F4) and parietal (P3 and P4) electrodes. The results revealed that the phase difference between the frontal electrodes (e.g., F3-F4) was close to 0 rad, suggesting consistent phase alignment in this region across frequencies. In contrast, pairs involving frontal and parietal electrodes (e.g., F3-P3, F3-P4) exhibited significant phase differences, which may indicate delayed interactions between the two regions. Notably, the AD patient

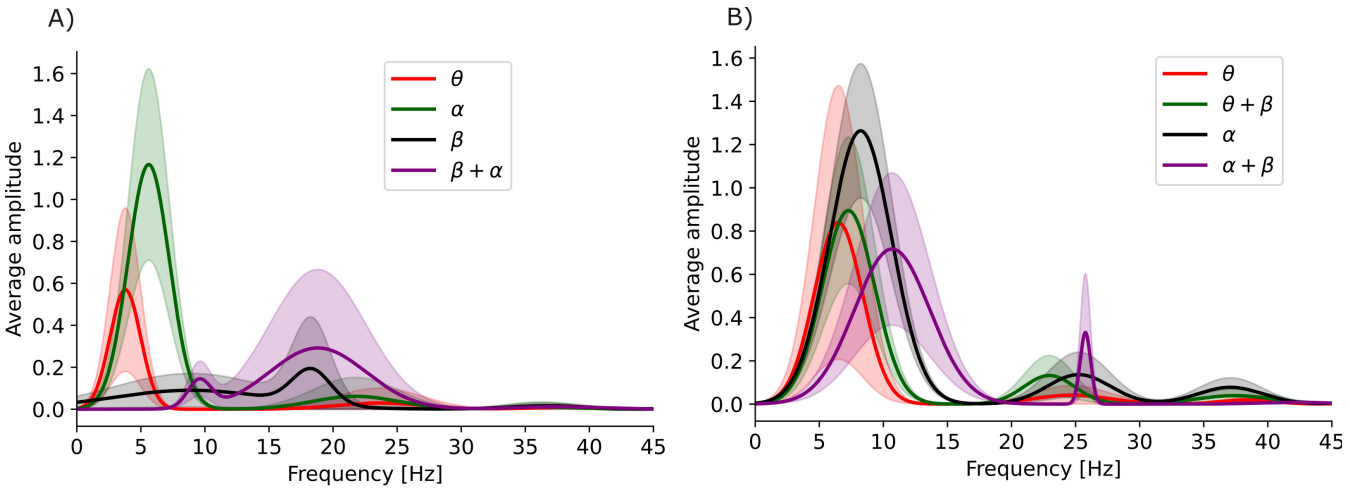

FIGURE 5. Spectral characterization of spontaneous brain activity using HsMM-SGP. A) Multi-mode oscillatory brain states inferred in the healthy control (HC). B) Multi-mode oscillatory brain states inferred in the Alzheimer's disease (AD) patient. The curves represent the average amplitude of the cross-spectra across channel pairs, and the shaded areas indicate ±2 std as a measure of variability around the average amplitude. The inferred states were labeled according to their amplitude within canonical frequency bands: theta (θ), alpha (α), beta (β), and gamma (γ). However, it is important to note that the states are not comparable across subjects.

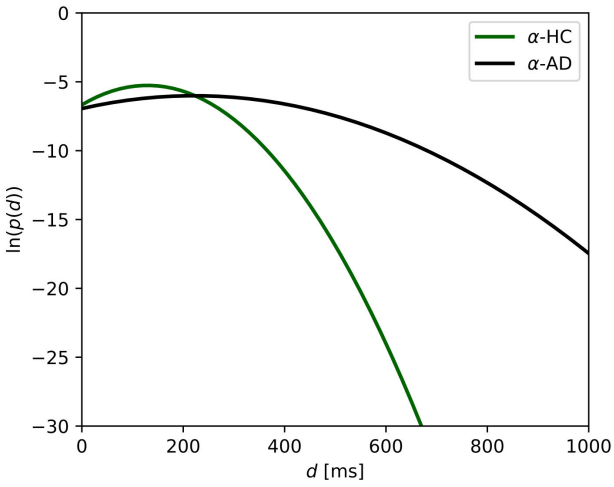

FIGURE 6. Logarithmic probability of duration for states labeled as α for the HC subject and the AD patient. The AD patient's α state shows a longer duration compared to the HC subject.

exhibited significant phase differences between frontal electrodes compared to the HC subject (see *Supplementary Material D*).

D. RELATION TO BIOPHYSICAL PARAMETERS

The distinct multi-mode oscillatory brain states between the HC subject and the AD patient raise the question of whether there is a relationship between the inferred states and biophysical parameters. This relationship could provide insights into variations in the underlying brain mechanisms across healthy and neurodegenerative conditions. To address this, the correlation between the PSD of the simulated signals and the PSD of the EEG data—averaged across all sensors—was computed for both subjects, for each pair of Kuramoto model parameters (W, MD). Each subject was then mapped to the point in the Kuramoto parameter space where the maximum correlation was achieved.

Fig. 8 shows the point for each subject on the heatmap of metastability, measured as the standard deviation of the Kuramoto order parameter. As shown in Fig. 8, the HC subject exhibited a stronger coupling (W) value and a shorter mean delay compared to the AD patient.

IV. DISCUSSION

We presented a generative model for estimating multi-mode oscillatory profiles of switching brain states from EEG data. The proposed model characterizes the spontaneous EEG data as continuous multi-output GP emissions driven by latent discrete states that evolve (switch) in time according to a semi-Markov process. The multi-output GP emissions are specified by multivariate spectral kernels, enabling the modeling of cross-covariance functions in the frequency domain. Multivariate spectral kernels represent mixtures of oscillatory modes, with mode-specific parameters that capture interactions at specific frequencies between channel pairs, including amplitude, spread, and phase shifts. Each state is associated with a multivariate spectral kernel that captures the spectral fingerprint of quasi-stationary time segments across a set of channels.

The dynamics of functional networks play a critical role in understanding healthy as well as pathological brain activity, providing insights into how different brain regions interact and coordinate to support cognitive and behavioral functions [52]. Disruptions in these dynamics are closely associated with a wide range of neurological and psychiatric disorders [53]. It is generally agreed that oscillatory processes play a fundamental role in the efficient coordination of large brain networks that underpin cognitive functions [23].

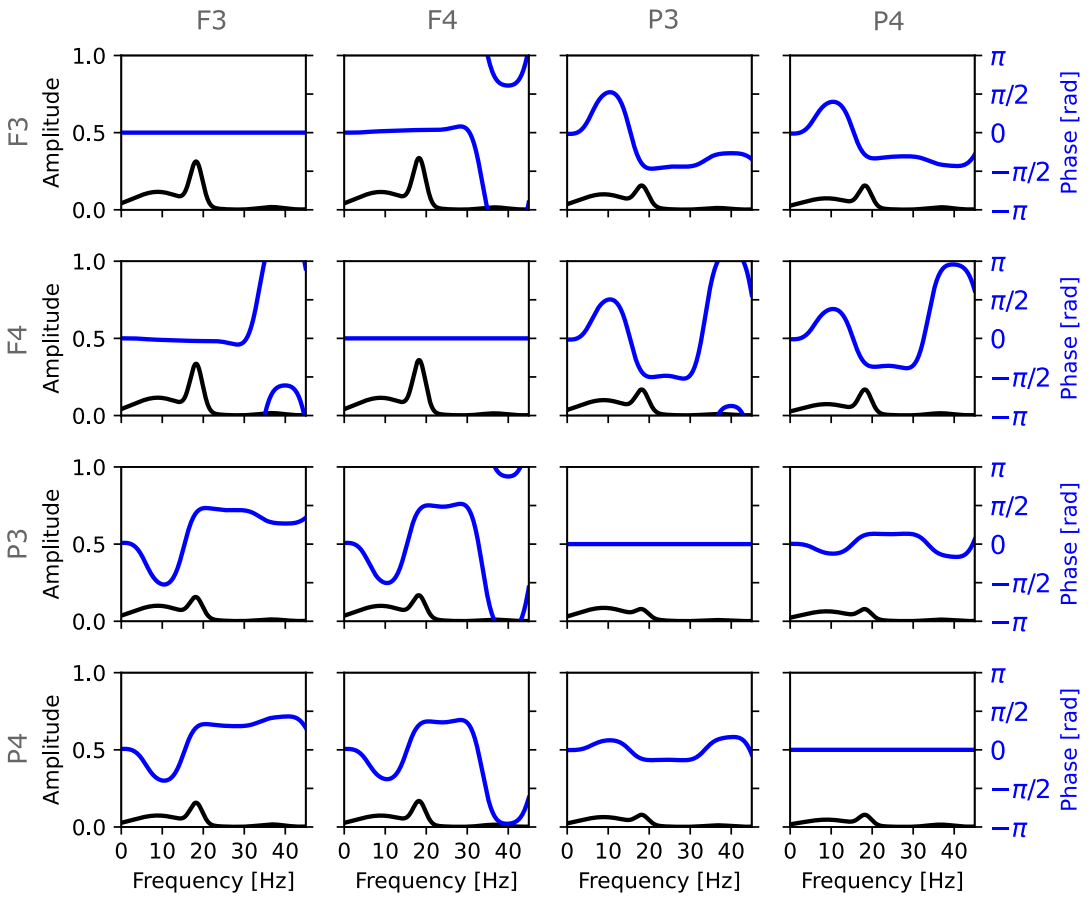

FIGURE 7. Cross-spectrum for an example state (β) of the HC subject. The cross-spectrum is shown for a subset of frontal (F3 and F4) and parietal (P3 and P4) channels. The black curves represent amplitude, and the blue curves represent phase differences, highlighting the phase alignment within the frontal region and the significant phase differences between the frontal and parietal regions.

A comprehensive spectral characterization of the brain's oscillatory states could provide insights into the mechanisms of neural coordination in both health and brain disorders.

Previous studies have proposed various approaches to characterize the spatio-temporal-spectral features of brain states in EEG data. The most widely used methods include sliding window analysis, Hidden Markov and Semi-Markov Models, matrix decomposition of windowed data, and the decomposition of functional connectivity matrices [14], [15]. However, some of these methods focused on characterizing the amplitude envelope of the recorded signals [9], [10], [54], were restricted to narrow frequency bands [31], or identified states dominated by a single frequency mode, limiting their ability to capture cross-frequency network interactions [32], [33], [34]. Various extensions of the HMM have been proposed that are capable of characterizing the spectral properties of brain states from raw electrophysiological data [19]. These approaches often leverage emission models that capture the historical temporal dependencies among observed data across different brain regions. Once the state time course is obtained, spectral estimation techniques are applied to the time segments where the state is active, providing estimates of the PSD for each state [20], [21].

In contrast to previous approaches, our model identifies multi-mode oscillatory brain states represented by a unique spectral 'fingerprint' from broadband oscillatory activity. This multi-mode oscillatory nature of states enables capturing interactions between local and global networks, which are crucial for coherent information processing across different brain regions. Furthermore, our model represents brain states using explicit spectral parameters that are directly estimated during the inference process, providing a more complete and realistic characterization of the underlying oscillatory processes. This approach effectively captures the transient nature of these processes, offering a more comprehensive and nuanced characterization of neural activity. Furthermore, allocating brain states with unique spectral 'fingerprints' allows for a better understanding of frequency-specific interactions, as well as the temporal organization of brain activity. These insights are crucial for advancing our understanding of brain function in both health and disease.

We validated the model using ground truth data generated from the HsMM-SGP generative model and from simulated

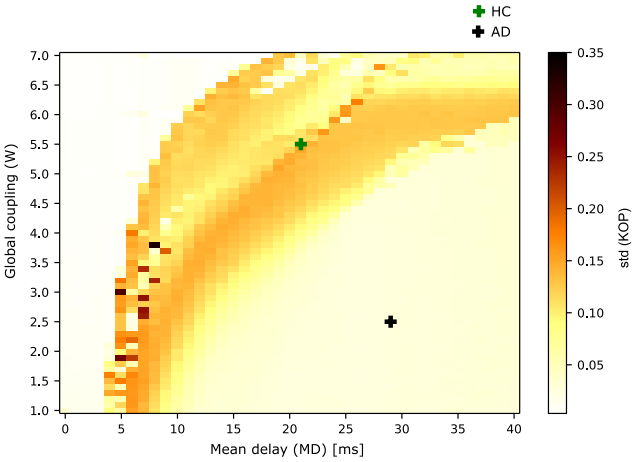

FIGURE 8. Approximation of the EEG power spectral densities from a healthy control (HC) subject and an Alzheimer's disease (AD) patient across a range of Kuramoto parameters. The heatmap shows the standard deviation of the Kuramoto order parameter (KOP) across a range of global coupling strength (*W*) and mean conduction delay (*MD*). The markers indicate the points in the Kuramoto parameter space where the maximum correlation for each subject was achieved.

brain-like activity using realistically coupled Kuramoto oscillators. Our results not only showed that the inference scheme effectively recovered the generative parameters, but also demonstrated the model's ability to infer multi-mode oscillatory states. Importantly, the inferred states meaningfully captured variations in emergent oscillatory dynamics driven by changes in structural biophysical parameters.

The practical application of the model was illustrated using EEG data from a healthy control subject and an AD patient. In both cases, the inferred brain states exhibited distinct spectral properties characterized by a dominant frequency within specific bands, along with background activity distributed across other canonical EEG bands. In particular, the multi-mode oscillatory brain states of the AD patient were dominated by lower frequencies. By comparison, control subjects exhibited a broader spectral range, with states characterized by prevalent modes in both low and high-frequency bands. These findings are consistent with the literature, where changes in the EEG spectrum in Alzheimer's disease have been consistently demonstrated to show increased power at lower frequencies, and reductions in both power and intra- and inter-hemispheric coherence in alpha and fast oscillations [27], [55], [56], [57]. Additionally, our results showed that the dissimilarity of the inferred multi-mode oscillatory states could be meaningfully related to biophysical parameters with biological interpretation, such as connectivity strength and conduction delay between brain regions. Recently, Cabral et al. [47] demonstrated using a phenomenological whole-brain network model that the emergent spatio-temporal-spectral properties of the whole system are critically modulated by variations in global coupling and delay. The model proposed here enables linking the properties of multi-mode oscillatory brain states to these structural parameters. This opens the opportunity for providing mechanistic explanations for observed EEG spectral abnormalities observed in brain disorders. Relating oscillatory brain states to mechanistic parameters could improve the interpretability of these states, and open new avenues for potential clinical applications, such as the early detection of brain disorders.

A. LIMITATIONS AND FUTURE WORK

Incorporating GPs as an emission model within the HsMM framework introduces computational challenges due to the complexity of estimating the model's hyperparameters. Standard GPs exhibit cubic time complexity, $O(T^3C^3)$ which limits scalability when handling multiple channels. This limitation can be addressed through approximate inference methods, such as sparse approximations. Furthermore, the inference process can be enhanced using approaches like Variational Bayes, which models uncertainty in the model parameters. This approach also provides a useful model order selection criterion by approximating the model evidence via the maximization of free energy. Future work should focus on incorporating these developments.

The present work can also be expanded to accommodate group-level inferences, specifically aiming to distinguish between healthy individuals and those under disease conditions. This could provide a deeper understanding of the neural dynamics associated with neurological and neuropsychiatric disorders.

V. CONCLUSION

In this work, a novel HsMM-SGP framework was introduced for modeling non-stationary brain states based on EEG data. The proposed model enables a fine-grained characterization of frequency-specific properties and their temporal evolution, making it particularly well-suited for analyzing non-stationary neural time series. Our method captures dynamic and complex interactions between oscillatory modes across channels, providing a more physiologically interpretable representation of brain activity. We conclude that the HsMM-SGP proposed here could be a valuable tool for advancing the understanding of brain dynamics in both health and disease.

REFERENCES

[1] F. Hancock, F. E. Rosas, P. A. M. Mediano, A. I. Luppi, J. Cabral, O. Dipasquale, and F. E. Turkheimer, "May the 4C's be with you: An overview of complexity-inspired frameworks for analysing resting-state neuroimaging data," *J. Roy. Soc. Interface*, vol. 19, no. 191, Jun. 2022, Art. no. 20220214. [Online]. Available: https://royalsocietypublishing.org/doi/abs/10.1098/rsif.2022.0214

[2] S. Cho, M. Van Es, M. Woolrich, and C. Gohil, "Comparison between EEG and MEG of static and dynamic resting-state networks," *Hum. Brain Mapping*, vol. 45, no. 13, p. 70018, 2024.

[3] K. J. Friston, "Functional and effective connectivity in neuroimaging: A synthesis," *Human Brain Mapping*, vol. 2, nos. 1–2, pp. 56–78, Jan. 1994. [Online]. Available: https://onlinelibrary.wiley.com/doi/abs/10.1002/hbm.460020107

[4] S. L. Bressler and V. Menon, "Large-scale brain networks in cognition: Emerging methods and principles," *Trends Cognit. Sci.*, vol. 14, no. 6, pp. 277–290, Jun. 2010. [Online]. Available: https://www.sciencedirect.com/science/article/pii/S1364661310000896

[5] P. M. Rossini, R. Di Iorio, F. Vecchio, M. Anfossi, C. Babiloni, M. Bozzali, A. C. Bruni, S. F. Cappa, J. Escudero, F. J. Fraga, P. Giannakopoulos, B. Guntekin, G. Logroscino, C. Marra, F. Miraglia, F. Panza, F. Tecchio, A. Pascual-Leone, and B. Dubois, "Early diagnosis of Alzheimer's disease: The role of biomarkers including advanced EEG signal analysis. Report from the IFCN-sponsored panel of experts," *Clin. Neurophysiol.*, vol. 131, no. 6, pp. 1287–1310, Jun. 2020. [Online]. Available: https://www.sciencedirect.com/science/article/pii/S1388245720300870

[6] L. Chouliaras and J. T. O'Brien, "The use of neuroimaging techniques in the early and differential diagnosis of dementia," *Mol. Psychiatry*, vol. 28, no. 10, pp. 4084–4097, Oct. 2023. [Online]. Available: https://www.nature.com/articles/s41380-023-02215-8

[7] C. M. Michel and T. Koenig, "EEG microstates as a tool for studying the temporal dynamics of whole-brain neuronal networks: A review," *NeuroImage*, vol. 180, pp. 577–593, Oct. 2018. [Online]. Available: https://www.sciencedirect.com/science/article/pii/S105381191731008X

[8] K. A. Severson, L. M. Chahine, L. A. Smolensky, M. Dhuliawala, M. Frasier, K. Ng, S. Ghosh, and J. Hu, "Discovery of Parkinson's disease states and disease progression modelling: A longitudinal data study using machine learning," *Lancet Digit. Health*, vol. 3, no. 9, pp. e555–e564, Sep. 2021. [Online]. Available: https://www.sciencedirect.com/science/article/pii/S2589750021001011

[9] N. J. Trujillo-Barreto, D. A. Galvez, A. Astudillo, and W. El-Deredy, "Explicit modeling of brain state duration using hidden semi Markov models in EEG data," *IEEE Access*, vol. 12, pp. 12335–12355, 2024.

[10] A. P. Baker, M. J. Brookes, I. A. Rezek, S. M. Smith, T. Behrens, P. J. Probert Smith, and M. Woolrich, "Fast transient networks in spontaneous human brain activity," *eLife*, vol. 3, p. 01867, Mar. 2014, doi: 10.7554/elife.01867.

[11] I. Olier, N. J. Trujillo-Barreto, and W. El-Deredy, "A switching multi-scale dynamical network model of EEG/MEG," *NeuroImage*, vol. 83, pp. 262–287, Dec. 2013. [Online]. Available: https://www.sciencedirect.com/science/article/pii/S1053811913003935

[12] A. Khanna, A. Pascual-Leone, C. M. Michel, and F. Farzan, "Microstates in resting-state EEG: Current status and future directions," *Neurosci. Biobehavioral Rev.*, vol. 49, pp. 105–113, Feb. 2015.

[13] C. Gohil, E. Roberts, R. Timms, A. Skates, C. Higgins, A. Quinn, U. Pervaiz, J. van Amersfoort, P. Notin, Y. Gal, S. Adaszewski, and M. Woolrich, "Mixtures of large-scale dynamic functional brain network modes," *NeuroImage*, vol. 263, Nov. 2022, Art. no. 119595.

[14] M. G. Preti, T. A. Bolton, and D. Van De Ville, "The dynamic functional connectome: State-of-the-art and perspectives," *NeuroImage*, vol. 160, pp. 41–54, Oct. 2017. [Online]. Available: https://www.sciencedirect.com/science/article/pii/S1053811916307881

[15] G. C. O'Neill, P. Tewarie, D. Vidaurre, L. Liuzzi, M. W. Woolrich, and M. J. Brookes, "Dynamics of large-scale electrophysiological networks: A technical review," *NeuroImage*, vol. 180, pp. 559–576, Oct. 2018. [Online]. Available: https://www.sciencedirect.com/science/article/pii/S1053811917308169

[16] P. Tewarie, L. Liuzzi, G. C. O'Neill, A. J. Quinn, A. Griffa, M. W. Woolrich, C. J. Stam, A. Hillebrand, and M. J. Brookes, "Tracking dynamic brain networks using high temporal resolution MEG measures of functional connectivity," *NeuroImage*, vol. 200, pp. 38–50, Oct. 2019. [Online]. Available: https://www.sciencedirect.com/science/article/pii/S1053811919304914

[17] O. Sporns, J. Faskowitz, A. S. Teixeira, S. A. Cutts, and R. F. Betzel, "Dynamic expression of brain functional systems disclosed by fine-scale analysis of edge time series," *Netw. Neurosci.*, vol. 5, no. 2, pp. 405–433, May 2021, doi: 10.1162/netn_a_00182.

[18] G. C. O'Neill, M. Bauer, M. W. Woolrich, P. G. Morris, G. R. Barnes, and M. J. Brookes, "Dynamic recruitment of resting state sub-networks," *NeuroImage*, vol. 115, pp. 85–95, Jul. 2015. [Online]. Available: https://www.sciencedirect.com/science/article/pii/S1053811915003213

[19] H. H. Larzabal, D. Araya, L. L. G. Rodriguez, C. Roman, N. Trujillo-Barreto, P. Guevara, and W. El-Deredy, "Efficient estimation of time-dependent brain functional connectivity using anatomical connectivity constraints," *IEEE Access*, vol. 11, pp. 50215–50234, 2023.

[20] D. Vidaurre, L. T. Hunt, A. J. Quinn, B. A. E. Hunt, M. J. Brookes, A. C. Nobre, and M. W. Woolrich, "Spontaneous cortical activity transiently organises into frequency specific phase-coupling networks," *Nature Commun.*, vol. 9, no. 1, p. 2987, Jul. 2018.

[21] D. Vidaurre, A. J. Quinn, A. P. Baker, D. Dupret, A. Tejero-Cantero, and M. W. Woolrich, "Spectrally resolved fast transient brain states in electrophysiological data," *NeuroImage*, vol. 126, pp. 81–95, Feb. 2016. [Online]. Available: https://www.sciencedirect.com/science/article/pii/S1053811915010691

[22] U. Pervaiz, D. Vidaurre, C. Gohil, S. M. Smith, and M. W. Woolrich, "Multi-dynamic modelling reveals strongly time-varying resting fMRI correlations," *Med. Image Anal.*, vol. 77, Apr. 2022, Art. no. 102366. [Online]. Available: https://www.sciencedirect.com/science/article/pii/S1361841522000196

[23] G. Buzsáki and A. Draguhn, "Neuronal oscillations in cortical networks," *Science*, vol. 304, no. 5679, pp. 1926–1929, Jun. 2004. [Online]. Available: https://www.science.org/doi/abs/10.1126/science.1099745

[24] M. Siegel, T. H. Donner, and A. K. Engel, "Spectral fingerprints of large-scale neuronal interactions," *Nature Rev. Neurosci.*, vol. 13, no. 2, pp. 121–134, Feb. 2012, doi: 10.1038/nrn3137.

[25] P. Fries, "A mechanism for cognitive dynamics: Neuronal communication through neuronal coherence," *Trends Cognit. Sci.*, vol. 9, no. 10, pp. 474–480, Oct. 2005. [Online]. Available: https://www.sciencedirect.com/science/article/pii/S1364661305002421

[26] M. Ursino and G. Pirazzini, "Theta–gamma coupling as a ubiquitous brain mechanism: Implications for memory, attention, dreaming, imagination, and consciousness," *Current Opinion Behav. Sci.*, vol. 59, Oct. 2024, Art. no. 101433. [Online]. Available: https://www.sciencedirect.com/science/article/pii/S2352154624000846

[27] M. S. Goodman, S. Kumar, R. Zomorrodi, Z. Ghazala, A. S. M. Cheam, M. S. Barr, Z. J. Daskalakis, D. M. Blumberger, C. Fischer, A. Flint, L. Mah, N. Herrmann, C. R. Bowie, B. H. Mulsant, and T. K. Rajji, "Theta-gamma coupling and working memory in Alzheimer's dementia and mild cognitive impairment," *Frontiers Aging Neurosci.*, vol. 10, p. 101, Aug. 2018. [Online]. Available: https://www.frontiersin.org/journals/aging-neuroscience/articles/10.3389/fnagi.2018.00101

[28] H. Brooks et al., "Theta–gamma coupling and ordering information: A stable brain–behavior relationship across cognitive tasks and clinical conditions," *Neuropsychopharmacology*, vol. 45, no. 12, pp. 2038–2047, Nov. 2020.

[29] M. S. Barr, T. K. Rajji, R. Zomorrodi, N. Radhu, T. P. George, D. M. Blumberger, and Z. J. Daskalakis, "Impaired theta-gamma coupling during working memory performance in schizophrenia," *Schizophrenia Res.*, vol. 189, pp. 104–110, Nov. 2017. [Online]. Available: https://www.sciencedirect.com/science/article/pii/S0920996417300579

[30] P. Prabhu, H. Morise, K. Kudo, A. Beagle, D. Mizuiri, F. Syed, K. A. Kotegar, A. Findlay, B. L. Miller, J. H. Kramer, K. P. Rankin, P. A. Garcia, H. E. Kirsch, K. Vossel, S. S. Nagarajan, and K. G. Ranasinghe, "Abnormal gamma phase-amplitude coupling in the parahippocampal cortex is associated with network hyperexcitability in Alzheimer's disease," *Brain Commun.*, vol. 6, no. 2, p. 121, Mar. 2024, doi: 10.1093/braincomms/fcae121.

[31] O. A. Heggli, I. Konvalinka, J. Cabral, E. Brattico, M. L. Kringelbach, and P. Vuust, "Transient brain networks underlying interpersonal strategies during synchronized action," *Social Cogn. Affect. Neurosci.*, vol. 16, nos. 1–2, pp. 19–30, Jan. 2021, doi: 10.1093/scan/nsaa056.

[32] B. W. Brunton, L. A. Johnson, J. G. Ojemann, and J. N. Kutz, "Extracting spatial–temporal coherent patterns in large-scale neural recordings using dynamic mode decomposition," *J. Neurosci. Methods*, vol. 258, pp. 1–15, Jan. 2016. [Online]. Available: https://www.sciencedirect.com/science/article/pii/S0165027015003829

[33] H. Jin, K. G. Ranasinghe, P. Prabhu, C. Dale, Y. Gao, K. Kudo, K. Vossel, A. Raj, S. S. Nagarajan, and F. Jiang, "Dynamic functional connectivity MEG features of Alzheimer's disease," *NeuroImage*, vol. 281, Nov. 2023, Art. no. 120358.

[34] N. Shettigar, C.-L. Yang, K.-C. Tu, and C. S. Suh, "On the biophysical complexity of brain dynamics: An outlook," *Dynamics*, vol. 2, no. 2, pp. 114–148, May 2022. [Online]. Available: https://www.mdpi.com/2673-8716/2/2/6

[35] C. E. Rasmussen and C. K. I. Williams, *Gaussian Processes for Machine Learning*. Cambridge, MA, USA: MIT Press, 2005, doi: 10.7551/mitpress/3206.001.0001.

[36] G. Parra and F. Tobar, "Spectral mixture kernels for multi-output Gaussian processes," in *Proc. 31st Int. Conf. Neural Inf. Process. Syst.* Red Hook, NY, USA: Curran Associates, 2017, pp. 6684–6693.

[37] K. R. Ulrich, D. E. Carlson, K. Dzirasa, and L. Carin, "GP kernels for cross-spectrum analysis," in *Proc. Adv. Neural Inf. Process. Syst.*, vol. 28, C. Cortes, N. Lawrence, D. Lee, M. Sugiyama, and R. Garnett, Eds., 2015, pp. 1–9.

[38] C. Torres-Valencia, Á. Orozco, D. Cárdenas-Peña, A. Álvarez-Meza, and M. Álvarez, "A discriminative multi-output Gaussian processes scheme for brain electrical activity analysis," *Appl. Sci.*, vol. 10, no. 19, p. 6765, Sep. 2020. [Online]. Available: https://www.mdpi.com/2076-3417/10/19/6765

[39] V. Caro, J.-H. Ho, S. Witting, and F. Tobar, "Modeling neonatal EEG using multi-output Gaussian processes," *IEEE Access*, vol. 10, pp. 32912–32927, 2022.

[40] S.-Z. Yu, *Hidden Semi-Markov Models: Theory, Algorithms and Applications*, 1st ed., Amsterdam, The Netherlands: Elsevier, 2015.

[41] A. Wilson and R. Adams, "Gaussian process kernels for pattern discovery and extrapolation," in *Proc. 30th Int. Conf. Mach. Learn.*, in Proceedings of Machine Learning Research, vol. 28, Atlanta, GA, USA, S. Dasgupta and D. McAllester, Eds., Jun. 2013, pp. 1067–1075. [Online]. Available: https://proceedings.mlr.press/v28/wilson13.html

[42] M. Stein, *Interpolation of Spatial Data: Some Theory for Kriging* (Springer Series in Statistics). New York, NY, USA: Springer, 2012.

[43] M. Gönen and E. Alpaydin, "Multiple kernel learning algorithms," *J. Mach. Learn. Res.*, vol. 12, pp. 2211–2268, Aug. 2011.

[44] M. A. Álvarez, L. Rosasco, and N. D. Lawrence, "Kernels for vector-valued functions: A review," *Found. Trends Mach. Learn.*, vol. 4, no. 3, pp. 195–266, 2012.

[45] S. L. Scott, "Bayesian methods for hidden Markov models," *J. Amer. Stat. Assoc.*, vol. 97, no. 457, pp. 337–351, Mar. 2002.

[46] J. Cabral, H. Luckhoo, M. Woolrich, M. Joensson, H. Mohseni, A. Baker, M. L. Kringelbach, and G. Deco, "Exploring mechanisms of spontaneous functional connectivity in MEG: How delayed network interactions lead to structured amplitude envelopes of band-pass filtered oscillations," *NeuroImage*, vol. 90, pp. 423–435, Apr. 2014.

[47] J. Cabral, F. Castaldo, J. Vohryzek, V. Litvak, C. Bick, R. Lambiotte, K. Friston, M. L. Kringelbach, and G. Deco, "Metastable oscillatory modes emerge from synchronization in the brain spacetime connectome," *Commun. Phys.*, vol. 5, no. 1, p. 184, Jul. 2022, doi: 10.1038/s42005-022-00950-y.

[48] N. Tzourio-Mazoyer, B. Landeau, D. Papathanassiou, F. Crivello, O. Etard, N. Delcroix, B. Mazoyer, and M. Joliot, "Automated anatomical labeling of activations in SPM using a macroscopic anatomical parcellation of the MNI MRI single-subject brain," *NeuroImage*, vol. 15, no. 1, pp. 273–289, Jan. 2002. [Online]. Available: https://www.sciencedirect.com/science/article/pii/S1053811901909784

[49] F. A. Torres, M. Otero, C. A. Lea-Carnall, J. Cabral, A. Weinstein, and W. El-Deredy, "Emergence of multiple spontaneous coherent subnetworks from a single configuration of human connectome coupled oscillators model," *Sci. Rep.*, vol. 14, no. 1, p. 30726, Dec. 2024.

[50] A. Miltiadous, K. D. Tzimourta, T. Afrantou, P. Ioannidis, N. Grigoriadis, D. G. Tsalikakis, P. Angelidis, M. G. Tsipouras, E. Glavas, N. Giannakeas, and A. T. Tzallas, "A dataset of scalp EEG recordings of Alzheimer's disease, frontotemporal dementia and healthy subjects from routine EEG," *Data*, vol. 8, no. 6, p. 95, May 2023.

[51] R. Krupnik, Y. Yovel, and Y. Assaf, "Inner hemispheric and interhemispheric connectivity balance in the human brain," *J. Neurosci.*, vol. 41, no. 40, pp. 8351–8361, Oct. 2021.

[52] G. Wu, Z. Cui, X. Wang, and Y. Du, "Unveiling the core functional networks of cognition: An ontology-guided machine learning approach," *NeuroImage*, vol. 298, Sep. 2024, Art. no. 120804. [Online]. Available: https://www.sciencedirect.com/science/article/pii/S105381192400301X

[53] Ö. Akgüller, M. A. Balcı, and G. Cioca, "Functional brain network disruptions in Parkinson's disease: Insights from information theory and machine learning," *Diagnostics*, vol. 14, no. 23, p. 2728, Dec. 2024. [Online]. Available: https://www.mdpi.com/2075-4418/14/23/2728

[54] N. Coquelet, X. De Tiège, L. Roshchupkina, P. Peigneux, S. Goldman, M. Woolrich, and V. Wens, "Microstates and power envelope hidden Markov modeling probe bursting brain activity at different timescales," *NeuroImage*, vol. 247, Feb. 2022, Art. no. 118850. [Online]. Available: https://www.sciencedirect.com/science/article/pii/S1053811921011216

[55] A. A. Flores-Sandoval, P. Davila-Pérez, S. S. Buss, K. Donohoe, M. O'Connor, M. M. Shafi, A. Pascual-Leone, C. S. Y. Benwell, and P. J. Fried, "Spectral power ratio as a measure of EEG changes in mild cognitive impairment due to Alzheimer's disease: A case-control study," *Neurobiol. Aging*, vol. 130, pp. 50–60, Oct. 2023. [Online]. Available: https://www.sciencedirect.com/science/article/pii/S0197458023001021

[56] A. M. van Nifterick, D. Mulder, D. J. Duineveld, M. Diachenko, P. Scheltens, C. J. Stam, R. E. van Kesteren, K. Linkenkaer-Hansen, A. Hillebrand, and A. A. Gouw, "Resting-state oscillations reveal disturbed excitation–inhibition ratio in Alzheimer's disease patients," *Sci. Rep.*, vol. 13, no. 1, p. 7419, May 2023, doi: 10.1038/s41598-023-33973-8.

[57] X. Chen, Y. Li, R. Li, X. Yuan, M. Liu, W. Zhang, and Y. Li, "Multiple cross-frequency coupling analysis of resting-state EEG in patients with mild cognitive impairment and Alzheimer's disease," *Frontiers Aging Neurosci.*, vol. 15, Aug. 2023, Art. no. 1142085. [Online]. Available: https://www.frontiersin.org/journals/aging-neuroscience/articles/10.3389/fnagi.2023.1142085

YUNIER PRIEUR-COLOMA received the B.Sc. degree in automatic engineering from Universidad de Oriente, Santiago de Cuba, Cuba, in 2016. He is currently pursuing the Ph.D. degree in health sciences and engineering with Universidad de Valparaíso, Valparaíso, Chile. His research interests include probabilistic modeling, computational neuroscience, machine learning, and biomedical signal processing.

FELIPE A. TORRES received the B.Eng. degree in electronics and telecommunications engineering from Universidad de Cuenca, Ecuador, in 2015, and the Ph.D. degree in electronics engineering from Universidad Técnica Federico Santa María, Chile, in 2021. He was a Postdoctoral Researcher at Universidad of Valparaíso, Chile. He is currently an Auxiliary Professor with the Departamento de Computación e Industrias, Universidad Católica del Maule, Chile. His research interests include computational neuroscience and control of neurostimulation.

NELSON J. TRUJILLO-BARRETO received the B.Sc. degree (Hons.) in nuclear physics from the Higher Institute for Nuclear Science and Technology, in 1995, and the Ph.D. degree in physical sciences from the University of Havana, Cuba, in 2006. From 1995 to 2014, he was with Cuban Neuroscience Centre, where he was also the Head of the Department for Brain Dynamics. Currently, he is a Reader (Associate Professor) in computational neuroscience with Manchester Metropolitan University, U.K.

WAEL EL-DEREDY received the B.Sc. degree in electrical and electronics engineering from Ain Shams University, Cairo, Egypt, the M.Sc. degree in electrical and electronics engineering from the Imperial College London, London, U.K., and the Ph.D. degree in neurocomputing from University College London, London. He is currently a Professor in computational neuroscience with Universidad de Valparaíso, Chile. His research interests include the probabilistic models of brain function, the development of novel methods for neuroimaging and application for neuroengineering, and neuroprostatics. His research is supported by MRC and EPSRC in the U.K., ANID Chile, and the Advanced Center for Electrical and Electronic Engineering, Chile.